Analysis Of Multiscale Corticomuscular Coupling Networks Based On Ordinal Patterns

Lantian Liu, Yunyuan Gao, Ming Meng, Michael Houston, and Yingchun Zhang

***Abstract*—The coupled analysis of corticomuscular function based on physiological electrical signals can identify differences in causal relationships between electroencephalogram (EEG) and surface electromyogram (sEMG) in different motor states. The existing methods are mainly devoted to the analysis in the same frequency band, while ignoring the cross-band coupling, which plays an active role in motion control. Considering the inherent multiscale characteristics of physiological signals, a method combining Ordinal Partition Transition Networks (OPTNs) and Multivariate Variational Modal Decomposition (MVMD) was proposed in this paper. The EEG and sEMG were firstly decomposed on a time-frequency scale using MVMD, and then the coupling strength was calculated by the OPTNs to construct a corticomuscular coupling network, which was analyzed with complex network parameters. Experimental data were obtained from a self-acquired dataset consisting of EEG and sEMG of 16 healthy subjects at different sizes of constant grip force. The results showed that the method was superior in representing changes in the causal link among multichannel signals characterized by different frequency bands and grip strength patterns. Complex information transfer between the cerebral cortex and the corresponding muscle groups during constant grip force output from the human upper limb. Furthermore, the sEMG of the flexor digitorum superficialis (FDS) in the low frequency band is the hub in the effective information transmission between the cortex and the muscle, while the importance of each frequency component in this transmission network becomes more dispersed as the grip strength grows, and the increase in coupling strength and node status is mainly in the γ band (30~60Hz). This study provides new ideas for deconstructing the mechanisms of neural control of muscle movements.**

***Index Terms*—Multivariate variational modal decomposition, ordinal partition transition networks, granger causality, functional corticomuscular coupling**

I. Introduction

ELECTROENCEPHALOGRAM (EEG) is an electrical signal collected on the surface of the scalp generated by the rhythmic activity of neuron clusters in the brain; surface Electromyogram (sEMG) is an electrical signal collected on the surface of the skin during the contraction of nerve-controlled muscles. During human movement, the rhythms of EEG and sEMG can reflect the body's sense of motor control and muscles. Studies have shown rhythmic synchronization between sEMG and EEG [1]. In human activity, the transmission of information between the cerebral cortex and muscles has both linear and non-linear properties [2], [3]. And there is both iso-frequency and cross-frequency coupling [4]. Studying the coupling between the sensorimotor cortex and muscles from a multiscale perspective allows the identification of links between control and sensory information from the cerebral cortex and response information from the associated muscles in different motor states at the same time, and the hierarchical nature of the coupling between EEG and sEMG can be explored. Research on the mechanisms of motor function control can be used to analyze the characteristics and musculature of muscle damage caused by brain diseases, which is of great value in the diagnosis, treatment, and assessment of the level of rehabilitation of motor neurological diseases.

EEG and sEMG are multiscale in both time domain and frequency. EEG contains information about cortical activity in a range of frequency bands, while sEMG exhibits different time-frequency domain characteristics in different muscle actions. Also, studies have shown that there is a nonlinear coupling between cortical and muscle surface electrical signals in the same and different frequency bands [5]. In order to investigate the correlation between coupling properties and frequency bands between EEG and sEMG, the wavelet decomposition [6] proposed by Qassim was introduced to study the coupling between EEG and sEMG. However, wavelet decomposition suffers from the limitation of wavelet basis and lacks the ability to perform adaptive decomposition based on the signals. To solve this problem, Huang proposed the concept

Manuscript submitted 28 September 2023. This work was supported in part by "Leading Goose" R&D Program of Zhejiang(2023C03026) , the National Nature Science Foundation of China (62371171, 61971168), Zhejiang Provincial Natural Science Foundation of China (LZ22F010003, Z23F030014). *(Corresponding author: Yunyuan Gao.)*

Lantian Liu is with the HDU-ITMO Joint Institute, Hangzhou Dianzi University, Hangzhou, China (e-mail: qzchwy@qq.com).

Yunyuan Gao is with the College of Automation, Hangzhou Dianzi University and the International Joint Research Laboratory for Autonomous Robotic Systems, Hangzhou, China (e-mail: gyy@hdu.edu.cn).

Ming Meng is with the College of Automation, Hangzhou Dianzi University, Hangzhou, China (e-mail: mnming@hdu.edu.cn).

Michael Houston is with the Department of Biomedical Engineering, University of Houston, Houston, USA (e-mail: mjhouston2@uh.edu)

Yingchun Zhang is with the Department of Biomedical Engineering, University of Houston, Houston, USA (e-mail: YZHANG94@uh.edu)

of Intrinsic Mode Functions (IMF) and the method of empirical mode decomposition [7], which is data-driven and adaptive. But it suffers from serious mode mixing [8] and is highly influenced by noise. Then Dragomiretskiy introduced the decomposition of the time series into the variational model and proposed a variational modal decomposition algorithm [9], which transformed the decomposition problem of the signal into the problem of finding the optimal solution of the variational model. On this basis, to process multi-channel timing signals simultaneously, Rehman proposed the Multivariate Variational Mode Decomposition (MVMD) [10] algorithm, which can obtain high-resolution time-frequency features while suppressing noise components. MVMD allows for the decomposition of multiscale signals into different modes, which helps to provide insight into signal interactions at different scales.

On the other hand, the methods for calculating the strength of coupling between time series have been improving. The traditional method of coherence [11] gives some characteristics of the functional connections between cortex and muscle during movement, but it cannot distinguish the directionality of information transfer in the motor nervous system. Afterwards, Granger proposed the Granger Causality (GC) analysis algorithm [12], which can compute causal relationships between time series in a directed manner and was applied in corticomuscular coupling analysis [13]. However, the linear coupling component and the nonlinear coupling component in the information transfer between the cerebral cortex and the response muscles coexist such that the linear analysis method can be extremely limited in terms of performance [14]. Afterwards, optimized nonlinear Granger causality has been proposed and continuously refined [15], [16], [17]. Staniek proposed the symbolic transfer entropy [18], [19] algorithm by exploiting the conditional mutual information in information theory. Then it was combined with methods of time series decomposition to parse the coupling between cortex and muscle at multiple levels [20], [21], [22]. But these methods cannot distinguish causal and non-causal interdependencies between two subsystems [23], which led to the proposal of Ordinal Partition Transition Networks (OPTNs) [24] algorithms for inferring causal links from multivariate time series.

To address the problem that existing coupling analysis methods cannot systematically analyze the causal links among multivariate EEG and sEMG, and to analyze the hierarchical nature of the coupling network, a multiscale corticomuscular coupling network analysis method combining MVMD and OPTNs has been proposed in this paper. The method takes advantage of OPTNs' ability to identify causal dependencies and suppress spurious coupling and MVMD data-driven simultaneous frequency-scale decomposition of multichannel signals. It can be used to analyze the characteristics of information exchange between cortical and muscles under different grip force patterns of human upper limb movements. The multilayer coupling network constructed by this method can reveal the variation of coupling characteristics among frequency bands more obviously, identify the causal links between multiple signals more accurately and detect the nonlinear coupling better, which is beneficial to explore the intrinsic connection between cortical and muscles and the mechanism of neural control of muscle in locomotion. Based on the advantages and characteristics of this method mentioned above, this study analyzes the characteristics and differences between different grip force patterns of human upper limb movements from the perspective of signal coupling using complex network parameter features. The contributions of this paper are mainly reflected in the following aspects.

(1) The results of identifying direct and indirect links between time series with OPTNs are more intuitive. Applying the OPTNs algorithm to calculate the coupling strength between EEG and sEMG can further characterize the differences in the causal links between signals across different patterns of human upper limb movements.

(2) MVMD has excellent characteristics in the scale decomposition of time series. The band mixing is mild when using MVMD for the scale decomposition of EEG and sEMG. Also, the algorithm is robust and can decompose the time series into multiple bands evenly according to the actual needs.

(3) Combined with the MVMD-OPTNs algorithm, the intrinsic causal links between EEG and sEMG signals were analyzed using a complex network approach, providing a new idea for systematic analysis of the information exchange between cortical and muscle during human upper limb movements.

II. Material And Methods

A. Framework

The framework of the research scheme in this paper is shown in Fig. 1. The EEG and sEMG are first preprocessed to remove artifacts and noise interference. Then the coupling strength between the two pairs of multi-band EEG and sEMG with OPTNs causal inference algorithm to verify the effectiveness of the method is calculated. The framework of the research scheme in this paper is shown in Fig. 1.

The EEG and sEMG are first preprocessed to remove artifacts and noise interference. Then calculate the coupling strength between the two pairs of multi-band EEG and sEMG with OPTNs causal inference algorithm to verify the effectiveness of the method. After that, we select suitable delay time and perform multiscale decomposition using MVMD for the full-band and low-band signals below 60 Hz, respectively, to investigate the changes of information transmission and the characteristics of information exchange between cortical muscles in the coupled functional network of human upper limb output brain myoelectricity.

B. Data Acquisition And Pre-processing

The experimental data used in this paper were obtained from a laboratory self-collected dataset containing data from a sample of 16 healthy subjects aged 24-26 years without any history of neurological impairment disease. The study followed the Declaration of Helsinki and was approved by the Ethics Committee of Hangzhou Mingzhou Naokang Rehabilitation Hospital. All participants signed an informed consent form and pledged not to have undergone similar experiments.

In this study, participants were arranged to sit in front of a screen in a sitting position, with their bodies as relaxed as possible, with both arms resting naturally on the armrests of the chair, holding a grip strength dynamometer. They then

completed 10 sets of 5kg, 10kg and 20kg gripping experiments with their left and right hands respectively, using standardized power grip in accordance with the movement and resting cues given by the equipment. Only steady state force output data were analyzed in this study, so in the experiment we ensured that subjects had achieved the required grip strength at the time of hitting the start tag and maintained this grip strength throughout the task. The experimental steps are shown in Fig. 2. Subjects cycled through resting and grasping maneuvers.

The 64-channel (NeuSen.W64, Neuracle, China) EEG signals and sEMG signals (Delsys Inc., Natick, MA, USA) were acquired simultaneously at a sampling frequency of 1000 Hz. In this study, sEMG of the brachioradialis (BR), flexor digitorum superficialis (FDS), flexor carpi radialis (FCR), flexor carpi ulnaris (FCU), biceps brachii(BB), triceps brachii (TB) were acquired from the right and left hands of healthy subjects. The EEG signals were pre-processed using the EEGLAB toolbox [22] and re-referenced using an average reference. A fourth-order Butterworth bandpass filter was then used to remove the baseline drift of the EEG and filter the noise between the typical frequency bands of EEG and sEMG. Then the interference of artifacts such as electrooculogram and electrocardiogram for the EEG signals was removed with Independent Component Analysis. Finally, the wavelet noise cancellation method was used for the EEG and sEMG respectively.

C. Causal Inference Based On OPTNs

In order to accurately identify causal links between time series, suppress spurious links, and detect nonlinear coupling, Ordinal Pattern (OP) is considered in this paper to be introduced into the calculation of coupling between EEG and sEMG for constructing multivariate OPTNs. OP is defined as the order of amplitude arrangement based on the time series, and the network it constructs is a Markov chain of time series in the phase space. For a given time series $X=\{x_c(t)\}_{t=1}^{T}$, the phase space trajectory reconstruction with embedding dimension m and lag d is performed according to Takens' embedding theorem [25], and the embedding vector is obtained as follows

$$v_c(t)=\{x_c(t),x_c(t+d),\cdots,x_c[t+(m-1)d]\},\quad t=1,2,\cdots,T-(m-1)d \tag{1}$$

Assuming that $a_s=(a_0,a_1,\cdots,a_{m-1})$ is an ordering of $(0,1,\cdots,m-1)$, the member $x_c(t),x_c(t+d),\cdots,x_c[t+(m-1)d]$ size ordering relation for the embedding vector $v_c(t)$ can correspond to a unique a_s that satisfies

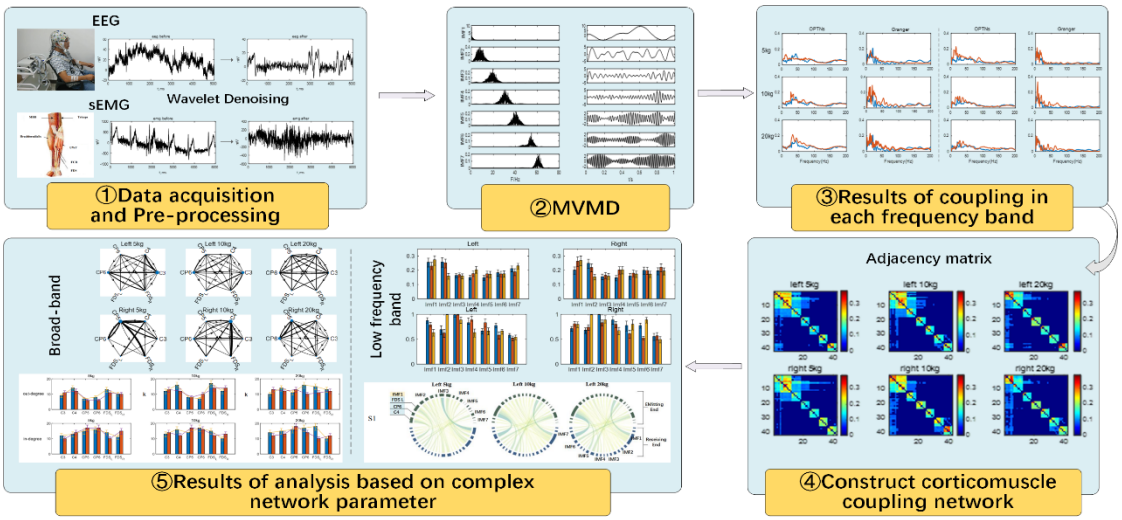

Fig. 1. Overview of the research process.

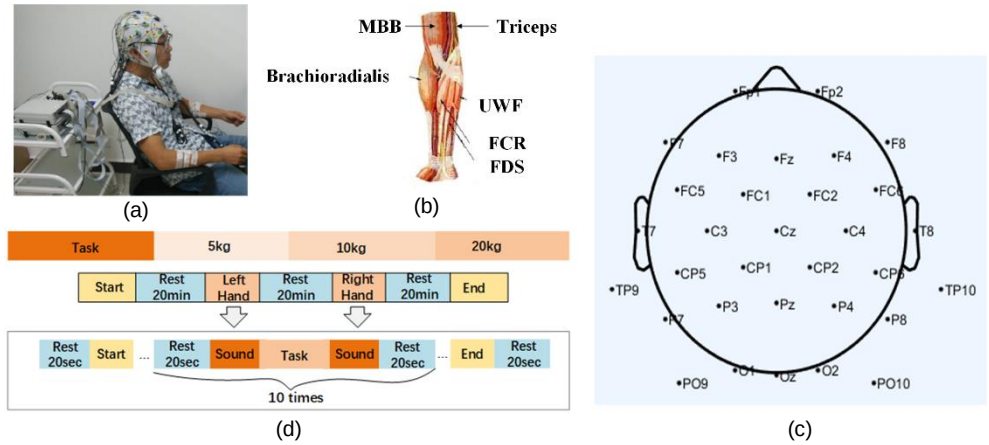

Fig. 2. (a) EEG-EMG simultaneous acquisition experiment;(b) Selection and placement of sEMG electrodes ;(c) Channal locations;(d) Flow of the experimental procedure.

$$x_c(t+a_0 d) \le x_c(t+a_1 d) \le \cdots \le x_c\left[t+a_{m-1} d\right] \tag{2}$$

And set $a_{l-1} < a_l$ when $x_c(t-a_{l-1}) = x_c(t-a_l)$. Each a_s is called an OP, and there exist m! different OP for the embedding dimension *m*. They are denoted by the symbol $\pi_1, \pi_2, \cdots, \pi_{M!}$.

The conditional entropy between time series is calculated and the *m*-OPTNs matrix is constructed. The conditional entropy of time series X_1 to X_2 at delay τ is formulated as follows

$$H_\tau(X_1 | X_2) = -\sum_{i=1}^{M!}\sum_{j=1}^{M!} p(\pi_j^{x_2,\tau}, \pi_i^{x_1}) \log_2 p(\pi_i^{x_1} | \pi_j^{x_2,\tau}) \tag{3}$$

$p(\pi_j^{x_2,\tau}, \pi_i^{x_1})$ denotes the frequency of simultaneous occurrence of $\pi_j^{x_2,\tau}$ and $\pi_i^{x_1}$. And $p(\pi_i^{x_1} | \pi_j^{x_2,\tau})$ indicates the conditional frequency of appearance of $\pi_i^{x_1}$ when OP mode $\pi_j^{x_2,\tau}$ occurs.

Similarly, the conditional entropy of time series X_2 to X_1 at delay τ is formulated as follows

$$H_\tau(X_2 | X_1) = -\sum_{i=1}^{M!}\sum_{j=1}^{M!} p(\pi_i^{x_1,\tau}, \pi_j^{x_2}) \log_2 p(\pi_j^{x_2} | \pi_i^{x_1,\tau}) \tag{4}$$

Construct the *m*-OPTNs matrix

$$H_\tau = \begin{bmatrix} H_\tau(X_1) & H_\tau(X_1|X_2) & \cdots & H_\tau(X_1|X_N) \\ H_\tau(X_2|X_1) & H_\tau(X_2) & \cdots & H_\tau(X_2|X_N) \\ \vdots & \vdots & \ddots & \vdots \\ H_\tau(X_N|X_1) & H_\tau(X_N|X_2) & \cdots & H_\tau(X_N) \end{bmatrix} \tag{5}$$

Set hard threshold as follows.

$$\hat{H}_\tau(X_n | X_m) = h_{nm\tau} = \begin{cases} H_{\max} & if\ H_\tau(X_n|X_m) \ge \lambda H_{\max} \\ H_\tau(X_n|X_m), & otherwise \end{cases} \tag{6}$$

$$H_{\max} = \log_2 M! \tag{7}$$

λ is empirically set to $0.99 \sim 1$. No link is considered to exist between two nodes when $\hat{H}_\tau(X_n | X_m)$ is set to $H_{\max}$.

It is crucial to ensure the accuracy of the causal link identification results and suppress the false links via the following three steps: determining the set of parents and children in the network; identifying the minimum set of neighbors between conditional action relations; removing the non-causal neighbors in the network. The pseudo links caused by indirect causal links in the causal analysis can be eliminated to ensure that the causal inference between the time sequences are valid links and the accuracy and effectiveness of the algorithm.

Step I: Find the parents and children of the network

By using OPTNs, for different delays $\left\{\tau_{p_1}, \tau_{p_2}, \cdots, \tau_{p_{km}}\right\}$, a weighted multilayer network $G = \{V, E\}$ is constructed based on the matrix $\hat{H} = \left\{\hat{H}_{\tau_1}, \hat{H}_{\tau_2}, \cdots, \hat{H}_{\tau_J}\right\}$. $V = \{X_1, X_2, \cdots, X_N\}$ represents the set of nodes of the weighted network. Treating each time series as a node, for different layers has the same set of nodes. $E = \{E_1, E_2, \cdots, E_J\}$ represents the set of edges of the weighted network, and the edges in the network are generally distinct for different layers.

For each node X_m in this multilayer network, its k_m parents can be found by the following equation.

$$\mathrm{P}_{X_m} = \left\{h_{mn\tau} \middle| h_{mj\tau} < H_{\max}, n \ne m, \tau \in T\right\} \tag{8}$$

$h_{mn\tau}$ represents the value of the *m*-th row and *n*-th column in the adjacency matrix $\hat{H}_\tau$. In other words, $h_{mn\tau}$ indicates the coupling strength value of the *m*-sequence for the *n*-sequence on the layer with delay τ in the multilayer weighted network. Similarly, the l_m children of X_m can be obtained from the following equation

$$C_{X_m} = \left\{h_{mn\tau} \middle| h_{in\tau} < H_{\max}, m \ne n, \tau \in T\right\} \tag{9}$$

Step II: Identify the minimum set of neighbors for conditioning

For the causality determination between X_m and X_n, define the minimum set of conditions

$$\mathrm{P}_{X_m}^{\min} = P_{X_m} \bigcap \hat{C}_{X_n} = \left\{p_1', p_2', \cdots, p_r'\right\} \tag{10}$$

$\hat{C}_{X_n}$ denotes the set of children of node X_n excluding X_m, i.e., $\hat{C}_{X_n} = C_{X_n} \setminus X_m$. The two special cases where *x* is the empty set are treated separately: set $\mathrm{P}_{X_m}^{\min} = \{X_m\}$ if X_m is the only child node of X_n; If $P_{X_m} \bigcap \hat{C}_{X_n} = \varnothing$, then set $\mathrm{P}_{X_m}^{\min} = P_{X_m} \bigcap P_{X_n}$, and if there is still no element in the minimal set of conditions, then set $\mathrm{P}_{X_m}^{\min} = \{X_m\}$. The most dominant set of neighbors can be filtered by setting an upper limit on the number of elements in the minimum set of conditions.

Step III: Remove non-causal neighbor nodes and fake links

To remove the effect of indirect causal links on the network analysis, we defined the parameters κ_{X_n} and $H\left(X_m \middle| P_{X_m}^{\min}\right)$ as follows.

$$\kappa_{X_n} = H\left(X_m \middle| P_{X_m}^{\min}\right) - H\left(X_m \middle| P_{X_m}^{\min}, X_n\right) \tag{11}$$

$$H\left(X_m \middle| P_{X_m}^{\min}\right) = -\sum_{i=1}^{M!}\sum_{j=1}^{M!} p(\pi_i^{p_1',\tau_1'}, \cdots, \pi_i^{p_r',\tau_r'}, \pi_j^{x_m}) \log p(\pi_j^{x_m} | \pi_i^{p_1',\tau_1'}, \cdots, \pi_i^{p_r',\tau_r'}) \tag{12}$$

κ_{X_n} can reflect the strength of the causal link between X_n and X_m to some extent. The more it tends to 0, the weaker the causal link of X_n to X_m, and the more likely the link is indirect. By setting a threshold value for κ_{X_n}, some indirect causal links in the network can be removed, and if $\kappa_{X_n} < \delta$, X_n will be regarded as a false link of X_m.

D. Multivariate Variational Modal Decomposition

MVMD is a data-driven time series scaling algorithm. The simultaneous frequency scaling decomposition of EEG and sEMG by using MVMD can consider the intrinsic connection between multivariate data. Also, the algorithm has excellent capability of frequency band division.

The purpose of the MVMD algorithm is to extract a specified number of *K* modulated oscillation vectors $u_k(t)$ from the input

data $x(t)=[x_1(t),x_2(t),\cdots,x_C(t)]$ of the c channels, with $x = b$, such that Ⅰ. the sum of the bandwidths of the extracted mode components is minimized; Ⅱ. the sum of the extracted mode components can accurately recover the original signal.

The analytic representation $u_+(t)$ of $u_k(t)$ is as follows.

$$u_+(t)=u(t)+j\mathrm{H}u(t)=\begin{bmatrix}u_+^1(t)\\u_+^2(t)\\\vdots\\u_+^C(t)\end{bmatrix}=\begin{bmatrix}a_1(t)e^{j\phi_1(t)}\\a_2(t)e^{j\phi_2(t)}\\\vdots\\a_C(t)e^{j\phi_C(t)}\end{bmatrix} \tag{13}$$

By estimating the bandwidth of each modulated oscillation vector $u_k(t)$ through the L_2 parametrization of the gradient function of $u_+(t)$, the cost function in the MVMD algorithm can be obtained as follows.

$$f=\sum_k\left\|\partial_t\left[e^{-j\omega_k t}u_+^k(t)\right]\right\|_2^2 \tag{14}$$

The bandwidth of the multivariate modulated oscillation is estimated by shifting the one-sided spectrum of all scales $u_+^k(t)$ by a single frequency component ω_k and taking the *Frobenius-2* parametrization. Then the cost function can be expressed by the following equation.

$$f=\sum_k\sum_c\left\|\partial_t\left[u_+^{k,c}(t)e^{-j\omega_k t}\right]\right\|_2^2 \tag{15}$$

Then the constrained optimization problem of the MVMD is expressed as

$$\begin{aligned}&\underset{\{u_{k,c}\},\{\omega_k\}}{\text{minimize}}\left\{\sum_k\sum_c\left\|\partial_t\left[u_+^{k,c}(t)e^{-j\omega_k t}\right]\right\|_2^2\right\}\\&s.t.\ \sum_k u_{k,c}(t)=x_c(t),c=1,2,\cdots,C\end{aligned} \tag{16}$$

The corresponding augmented Lagrangian function is

$$\begin{aligned}L(\{u_{k,c}\},\{\omega_k\},\lambda_c)&=\alpha\sum_k\sum_c\left\|\partial_t\left[u_+^{k,c}(t)e^{-j\omega_k t}\right]\right\|_2^2\\&+\sum_c\left\|x_c(t)-\sum_k u_{k,c}(t)\right\|_2^2+\sum_c\left\langle\lambda_c(t),x_c(t)-\sum_k u_{k,c}(t)\right\rangle\end{aligned} \tag{17}$$

ADMM is used to solve the unconstrained optimization problem, which simplifies the problem by transforming the complex optimization problem into multiple suboptimization problems.

Step Ⅰ: Mode update

Considering the mode update, this Lagrangian function can be equivalently transformed into the following optimization problem.

$$\begin{aligned}u_{k,c}^{n+1}=\arg\min_{u_{k,c}}\Bigg\{&\alpha\left\|\partial_t\left[u_+^{k,c}(t)e^{-j\omega_k t}\right]\right\|_2^2\\&+\left\|x_c(t)-\sum_i u_{i,c}(t)+\frac{\lambda_c(t)}{2}\right\|_2^2\Bigg\}\end{aligned} \tag{18}$$

The frequency domain update relation in MVMD can be obtained as follows

$$\hat{u}_{k,c}^{n+1}(\omega)=\frac{\hat{x}_c(\omega)-\sum_{i\neq k}\hat{u}_{i,c}(\omega)+\frac{\hat{\lambda}_c(\omega)}{2}}{1+2\alpha(\omega-\omega_k)^2} \tag{19}$$

Step Ⅱ: Center frequency update

Consider the optimization problem of central frequency update. Since the last two terms of the Lagrangian function are independent of ω_k, the central frequency update scheme is given by the following optimization problem.

$$\omega_k^{n+1}=\arg\min_{\omega_k}\left\{\sum_c\left\|\partial_t\left[u_+^{k,c}(t)e^{-j\omega_k t}\right]\right\|_2^2\right\} \tag{20}$$

The above equation can be equivalently transformed with Plancherel's theorem. The equation for the center frequency update is obtained as follows.

$$\begin{aligned}\omega_k^{n+1}&=\arg\min_{\omega_k}\left\{\sum_c\int_0^\infty(\omega-\omega_k)^2\left|\hat{u}_{k,c}(\omega)\right|^2d\omega\right\}\\&=\frac{\sum_c\int_0^\infty\omega\left|\hat{u}_{k,c}(\omega)\right|^2d\omega}{\sum_c\int_0^\infty\left|\hat{u}_{k,c}(\omega)\right|^2d\omega}\end{aligned} \tag{21}$$

E. Multiscale Corticomuscular Coupling Network Construction

In the construction of the corticomuscular coupling network, each sampled channel is used as the node of the network, and the weights in the multilayer weighted network calculated by OPTNs are used as the edges of the network. For each IMF obtained using MVMD decomposition, the weights of the optimal delay are selected as the coupling strength to construct the adjacency matrix. And the multilayer cerebral myoelectric signal coupling network is built based on the adjacency matrix.

The use of graph theory to characterize the topological relationships of complex networks is an important tool to study the different nodes, edges and the overall properties of the network [26]. In this paper, we use several network parameters in complex networks, such as node degree, node strength, mediator [27], agglomeration coefficient [28] and characteristic path length [29] to analyze the coupling properties between EEG and sEMG among different scales from the network level and node level. These parameters allow the topology of the network to be portrayed, to demonstrate more graphically the characteristics of information transmission in the coupled network, and to understand the myoelectricity of the coupling connection transformation between EEG and sEMG when a constant grip force is output from the human upper limb from a multilevel scale.

III. RESULTS

A. Analysis Of Corticomuscular Coupling In Each Frequency Band Based On OPTNs

The coupling of EEG and sEMG in each frequency band under continuous output of 5kg, 10kg and 20kg grip force of human upper limbs was calculated using OPTNs causal inference algorithm and Granger causal inference algorithm according to the above method. Then we compared the results obtained by using each of the two methods, and the results are shown below.

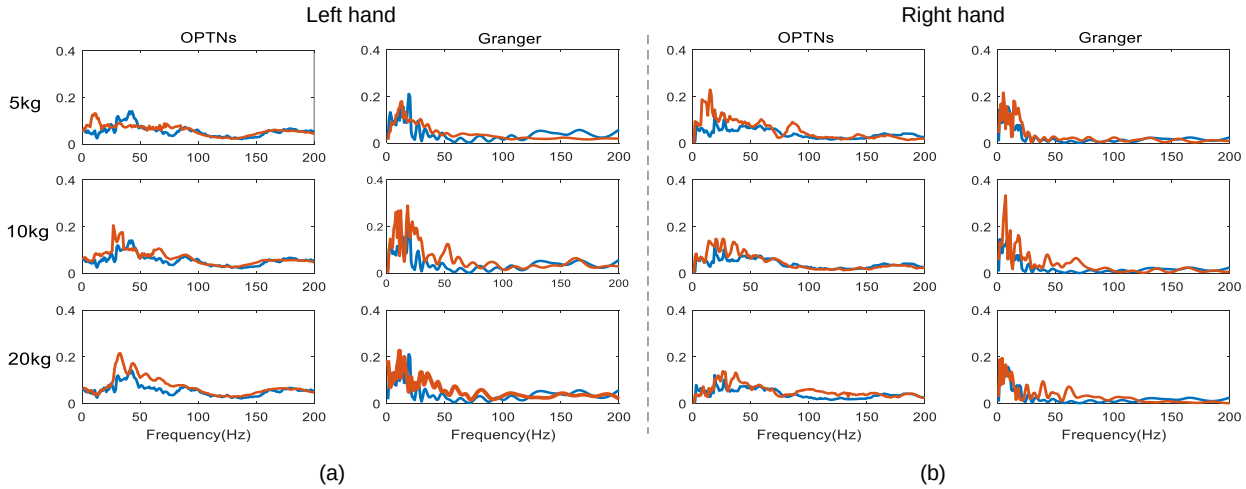

Fig. 3. Coupling intensity values between EEG and sEMG in each frequency band at 5kg, 10kg and 20kg grip force output for the right and left hands (a) Left hand (b) Right hand

The three images on the left side in Fig. 3 represent the calculated results of coupling strength at 5 kg, 10 kg and 20 kg grip force of left hand calculated using OPTNs and Granger causal inference algorithm, respectively. And the graphs on the right side indicate the coupling results of right hand. The blue lines in the figure indicate the significance threshold, and the red lines indicate the calculated results of the coupling. It can be seen that both methods exhibit changes in the synchronous coupling relationship between cortex and muscle across frequency bands. Besides, the calculation results of coupling strength using both algorithms have similar trends. As the grip force magnitude rose, the peak of coupling intensity in the EEG →EMG direction shifted from α (8-13 Hz) to γ (35-60 Hz) band. The coupling strength in the high-frequency range also shows a slight increase. All the above findings are consistent with the existing studies [30]-[37].

Comparing the result plots of the two methods, it can be seen that the OPTNs method has a larger significant region on the coupling curve than Granger method. Secondly, in the high frequency band, the coupling curves calculated by the OPTNs reflect the coupling curves at constant output grip. The coupling curves in the resting state basically overlap, and there is basically no significant region. But the two curves obtained by the Granger method have several crossings and peaks in the high frequency band many times. Also, GC still exhibits significant regions in the high-frequency range above 100Hz, although this is not the primary frequency range of EEG signals. Moreover, the coupling strength calculated by OPTNs method has a smaller variance between multiple trials and the results are more stable. The results indicate that the OPTNs has advantages over the GC in the detection of coupling features and can demonstrate the differences of coupling between frequency bands more obviously.

B. Simultaneous Frequency Scale Decomposition Of EEG And sEMG

MVMD allows simultaneous frequency-scale decomposition of EEG and sEMG. It was performed on the EEG and sEMG of all subjects after pre-processing, and the C3, C4, CP5, CP6 and the left and right superficial FDS channels associated with human upper limb fist movements were selected for analysis. The preset number of IMF k was determined by the center frequency observation method, and the appropriate bandwidth was set to select the center frequency that meets the requirements. The decomposition results of each component will be displayed in Fig. 4. IMF1~IMF6 (0-18Hz, 18-50Hz, 50-71Hz, 71-88Hz, 88-116Hz, 116-152Hz) are selected as the main frequency bands. The left panel shows the spectrogram of each component, and the right panel shows the corresponding IMF. It can be seen that there is basically no band mixing between the modes obtained from the decomposition, and the smoothness of each component is also well.

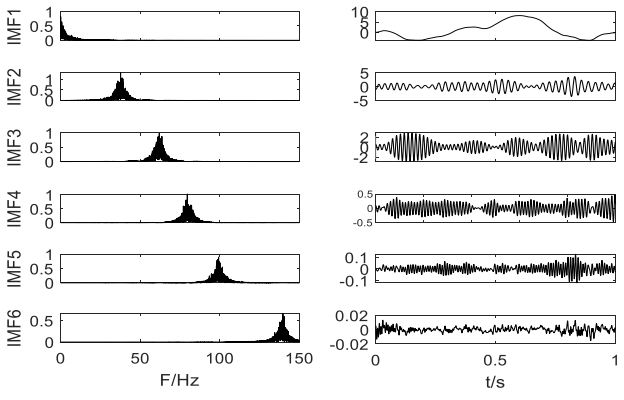

Fig. 4. MVMD decomposition results of C4 channel (a) Frequency spectrum of each IMF component (b) Time domain waveform of each IMF component.

C. Results Of Broad-band Cortical Muscle Coupling Network Analysis

We have calculated the coupling adjacency matrix among the IMFs of EEG and sEMG according to the OPTNs algorithm introduced above. The adjacency matrix between the channels calculated at each scale is shown in the following figure for subject S1 as an example.

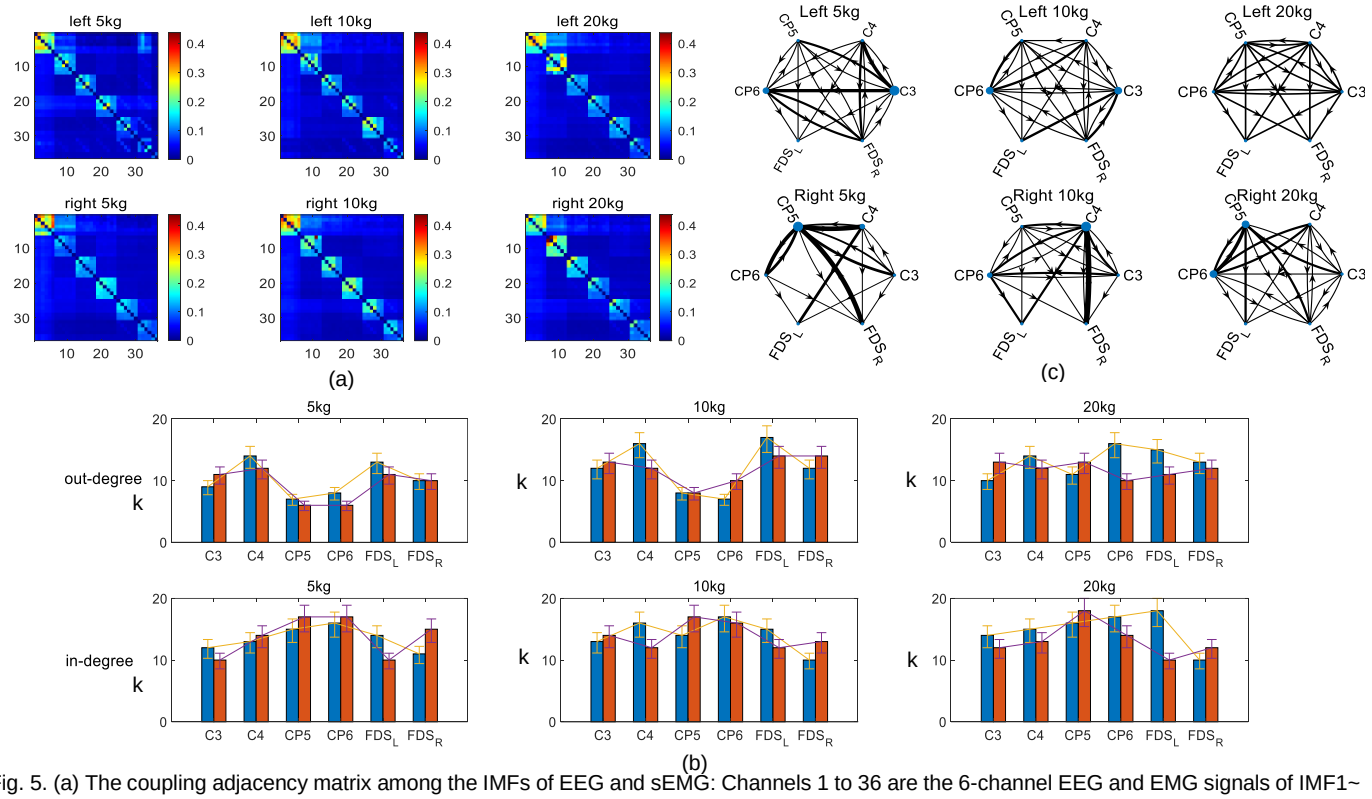

Fig. 5. (a) The coupling adjacency matrix among the IMFs of EEG and sEMG: Channels 1 to 36 are the 6-channel EEG and EMG signals of IMF1~IMF6, respectively, where channels 1 to 6 are the 6-channel EEG signals at the IMF1 level, and so on. (b) Network parameters of corticomuscular coupling network: Nodal degrees, blue: left hand, red: right hand. (c) Network parameters of corticomuscular coupling network: Edge mediators and node mediators: the thicker edges in the network reflect that the edge has a higher edge mesonumber and the nodes with larger node mesonumbers have larger diameters

The cross-coupling adjacency matrix between the frequency bands is shown in Fig. 5 (a). The figure shows that when the left hand outputs a sustained grip, the node that outputs information externally is mainly the C4, while the EMG channel that outputs and receives information is mainly the FDS of the left hand, and the EEG channel that receives information is mainly the CP6. When the right hand outputs sustained grip force, the control signal is mainly output by the C3, which controls the right FDS and transmits the information to the CP5 in sensory area. This reflects the bidirectional transmission of information between the cerebral cortex and the controlled muscles, moreover, it verifies that the coupling strength in the downward direction is higher than that in the upward direction of the corticomuscular coupling [38]-[41].

Furthermore, the coupling intensity between channels at the same scale was significantly stronger than that between signals at different scales at constant grip output from the hand. At constant force output, the peak of coupling intensity between EEG and sEMG channels appeared in the low frequency band. In the IMF3 band, there was a slight boost in the coupling intensity, and that in IMF5 and IMF6 also rose with the increasing grip force.

In Fig. 5(b), at each level of grip strength, the in-degree of C3 and C4 channels was larger, while the out-degree of CP5 and CP6 channels was larger. There were significant differences between left and right hands ($p>0.05$). In the left hand experiment, C4 and CP6 channels showed more obvious performance, while C3 and CP5 channels showed more obvious performance in the right hand experiment. And the controlled muscles in the right hand grasp experiment can be found to be mainly the FDS of the right hand, but in the left hand grasp experiment, the FDS of both hands have larger outward and inward degrees, which may be related to the right-handedness of the subjects. Fig. 5(c) shows edge mediators and node mediators of the network. The resultant plots show that the EEG nodes have a larger role and influence in the network. As the grip force increases, more information transmission between channels is activated and the roles and influences played by each node in the network are more evenly distributed. And the experiments show that the information circulation speed of the full-band EEG coupled network under each grip force of the left and right hands is not much different.

D. Results Of Low-band Cortical Muscle Coupling Network Analysis

In the above experiments, it can be seen that there is a high coupling strength between the EEG signals in the low frequency band. So further multiscale coupling networks were constructed for EEG and sEMG below 60 Hz to analyze the variations in the information exchange of the low frequency band. The signal is decomposed using MVMD, and seven IMF components are derived sequentially according to the center frequency selection method: 0-3Hz, 3-11Hz, 11-25Hz, 20-40Hz, 33-47Hz, 47-59Hz, and 55-65Hz.

The cross-coupling relationships among multiscale EEG and sEMG signals in the low frequency band are shown in Fig. 6. It can be seen from the figure that the coupling phenomenon is more obvious between the same scales. And the coupling

intensity tends to shift to the high frequency band as the grip force increases. The trend is the same for the left and right hands. For IMF1, there is a strong coupling between signals. For IMF2, the coupling strength decreases as the grip force increases. Coupling strength in IMF4 increases as the grip force increases. Where IMF2 largely overlaps with the α band, IMF3 largely overlaps with the β band, IMF4 and IMF5 largely contain the γ band, and the β and γ bands are thought to represent cortical transfer to the muscular system in terms of neural oscillations swhen static force is adjusted to dynamic force output [42].

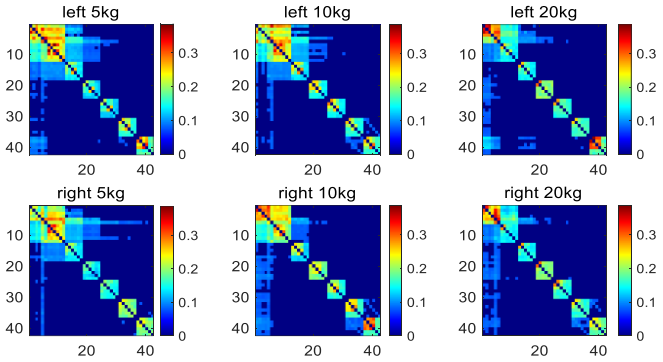

Fig. 6. Low frequency band corticomuscular coupling adjacency matrix: Channels 1 to 42 are the 6-channel EEG and EMG signals from IM` F1 to IMF7, respectively. Channels 1 to 7 are the 6-channel EEG signals of IMF1, and so on.

For the left-hand and right-hand experiments, the C4, CP6, left FDS channel and the C3, CP5, right FDS channel were selected for analysis, the results of which were found to be consistent in the experiments. The results of the following coupling analysis were chosen as an example for the left-handed experimental results.

The node intensities and mediators of the coupled networks at different scales are shown in Fig. 7. It can be seen in Fig. 7 (a) and (b) that the low-band signal has larger nodal intensities inside and outside the node at a constant grip force output. The IMF1 of FDS has larger nodal strength when the grip force is small, while as the grip force increases it decreases. IMF3 and IMF4 nodal intensities are smaller, while IMF6 and IMF7 nodal intensities have increased. There was a significant enhancement of information exchange between IMF4 and other channels as the grip force increased, which might be attributed to the activation of information exchange between cortical muscles in the high frequency band when the grip force increased. The network edge median chord diagram of multiple subjects showed a similar trend, reflecting the influence of the coupling relationship between signals of different scales in the network. Fig. 7 (c) displays the network edge median chord diagram for S1 subjects. It can be seen that the IMF1 and IMF7 components have more significant influence in the network, especially the IMF1 component of the myoelectric channel, and the importance of the connected edges of the nodes in the coupled network changes with the changing of the grip force. Moreover, the edge betweenness centrality of EEG nodes as emitting ends should be greater than that of receiving ends, indicating that EEG nodes tend to emit signals more frequently.

IV. Discussion

A. Characteristics Analysis Of MVMD-OPTNs Algorithm Based On Results

Based on MVMD and OPTNs, we quantitatively analyzed the causal relationship between EEG and sEMG in human upper limbs with constant grip force output. We also analyzed the coupling functional network consisting of EEG and sEMG channels using complex network parameters. Simultaneous frequency-scale decomposition of EEG and sEMG can be performed using MVMD. The method can eliminate the spectral overlap between frequency bands by setting the bandwidth and has a small transient frequency fluctuation and is robust. This is the verified advantageous time-frequency scale decomposition method for time series used so far. Using OPTNs to calculate the coupling strength compared with GC, the coupling strength varies more significantly between

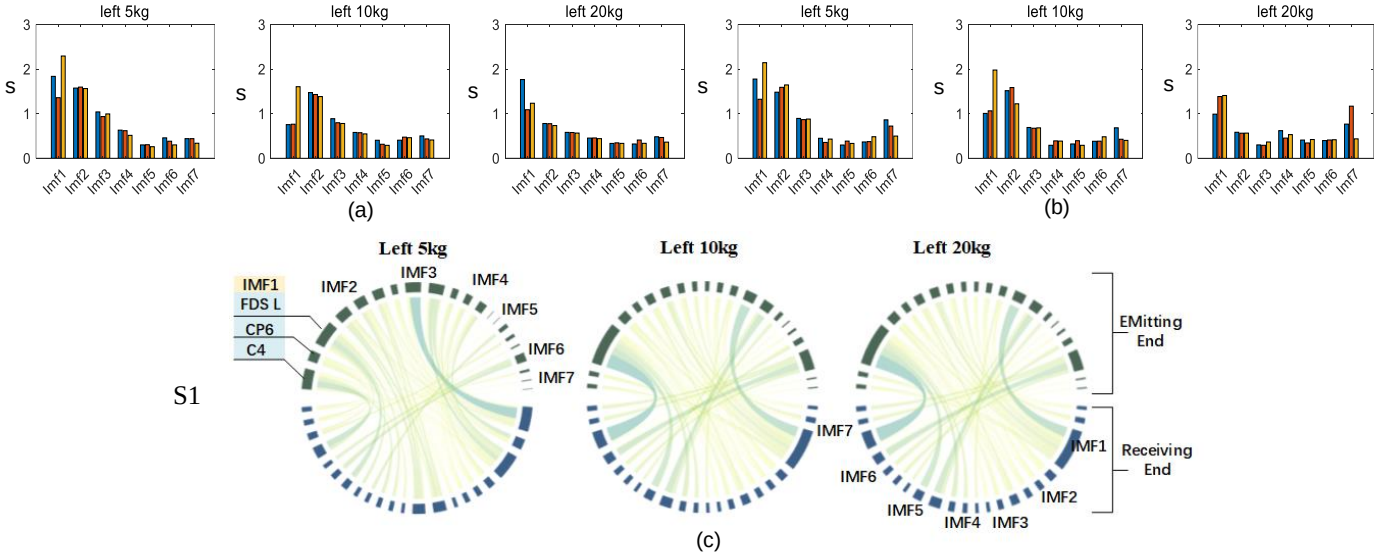

The upper half of the network edge mesoscope chord diagram shows the emitting end and the lower half shows the receiving end. The horizontal coordinates in the figures are the IMF1 component of the three-channel signal from left to right up to the IMF7 component of the three-channel signal.

Fig. 7. Network parameters of corticomuscular coupling network for each IMF (a) Internal strength; (b) External strength; (c) Mediators: the thicker edges in the network reflect that the edge has a higher edge mediator and the nodes with larger node mediator have larger area.

frequency bands. Moreover, OPTNs takes multiple channel inputs into consideration when calculating the coupling intensity, which is more conducive to analyzing the changes of coupling characteristics among the scales of EEG and sEMG under different grip force patterns of upper limb movements and makes the construction of coupling networks more reasonable.

B. Network Characteristics Of The Sensorimotor System

Nodes with a critical role in a complex network are not only related to their central location, but also to the timing of information exchange with other nodes [43], [44]. In the coupled cortical-muscular function network of human upper limb movements, the C3 and C4 play a critical role in information sending, while the FDS of the left and right hands receive signals while sending them. Information transmission between the cerebral cortex and the muscles is bidirectional. The cerebral cortex outputs a large amount of information when it controls the movement of muscles in the motor area. Human activity is also performed by multiple muscles in concert, and there are coupling associations among sEMG signals from different locations.

In the crossband experiments, in the high-frequency band, the peak coupling between EEG and sEMG occurs between simultaneous frequency scales. The coupling intensity in the high frequency band increased in the case of increasing grip force. During the experiments in the low frequency band, it was found that there was a strong coupling between the low frequency band sEMG (IMF1) and EEG, and that the low frequency band EMG channels assumed an important role in the transmission of information in this directed network. As the grip level rises, the higher frequency band (IMF4, IMF6) EEG and sEMG components have an increased position in the information transmission in this coupled network. These scale components are mainly gamma bands, which are consistent with the transfer characteristics of the cerebral cortex to the muscular system in terms of neural oscillations during static force adjustment to dynamic force output. Moreover, the coupling networks at the IMF2 and IMF3 scales have faster information transfer and better connectivity at static force output, which also suggests that there are differences in neural pathways at different scale components during constant grip force output from human upper limb movements.

C. Global Network Parameter Analysis

Two network parameters, the characteristic path length and the agglomeration coefficient, are shown in Figs. 8 (a) and (b) for the corticomuscular coupling network during human upper limb movements at each scale for the three grip force patterns, respectively. Blue represents 5 kg grip force, red represents 10 kg grip force, and yellow represents 20 kg grip force. The characteristic path length is shorter at the IMF3 and IMF4 scales, indicating faster information flowing. In Fig. 8, it shows that the IMF2 and IMF3 scales have larger clustering coefficients, and there is consistency between the left and right hands, suggesting that the signal coupling is tighter and has better connectivity at this scale. However, the information flow speed and connectivity of the network did not show a clear pattern of change with the variation of grip force level. The significance test shows that the network parameters are significantly different between the three grip strength patterns($p<0.05$) in several IMFs.

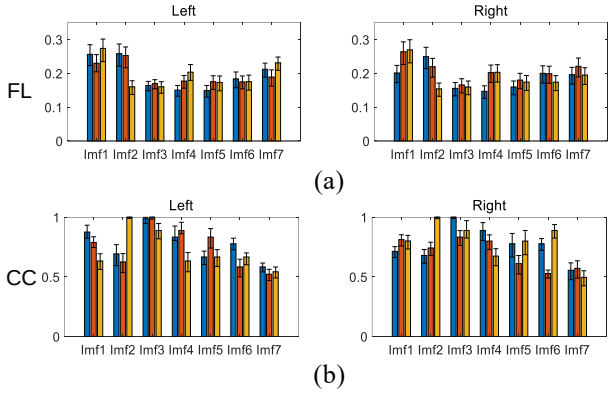

Fig. 8. Network parameters of corticomuscular coupling networks at each scale: (a) Feature path length; (b) Clustering coefficients.

V. Conclusion

To address the problems that traditional coupling methods cannot perform multiscale simultaneous analysis of multidimensional time-series signals and have certain limitations in describing coupling characteristics, we propose a complex network analysis method based on MVMD and OPTNs causal inference method. The method models the corticomuscular information transfer system from a holistic perspective and evaluates the coupling characteristics between EEG and sEMG at different scales of human upper limb movements through complex network parameters. The results show that the vital information transmission nodes in the network are consistent at different time-frequency scales. However, there are some variabilities in the coupling network at different scales, and stronger coupling properties exist between signals in the lower frequency bands. The complex network analysis method portrays the degree of importance of signals at different scales in the information exchange between cortex and muscle, which can provide a reasonable explanation for the variation of the coupling strength among scales of multidimensional EEG and sEMG. But the method still needs wider validation and application to ensure its applicability to different clinical and research scenarios. Also, how the network parameters in the method are specifically related to biological processes needs to be further explored, which will contribute to a deeper understanding of neural control and rehabilitation mechanisms. This research may contribute valuable insights for designing biomedical engineering devices and technologies, such as neuroprosthetics or brain-machine interfaces.

References

[1] B. Conway et al., "Synchronization between motor cortex and spinal motoneuronal pool during the performance of a maintained motor task in man.," The Journal of physiology, vol. 489, no. 3, pp. 917–924, 1995.

[2] X. Ping, Y. Fang-Mei, L. Xin-Xin, Y. Yong, C. Xiao-Ling, and Z. Li-Tai, "Functional coupling analyses of electroencephalogram and electromyogram based on variational mode decomposition-transfer entropy," Acta Physica Sinica, vol. 65, no. 11, 2016.

[3] N. Sinha, J. P. Dewald, C. J. Heckman, and Y. Yang, "Cross-frequency coupling in descending motor pathways: Theory and simulation," Frontiers in Systems Neuroscience, vol. 13, p. 86, 2020.

[4] Y. Yang, T. Solis-Escalante, J. Yao, F. C. Van Der Helm, J. P. Dewald, and A. C. Schouten, "Nonlinear connectivity in the human stretch reflex assessed by cross-frequency phase coupling," International journal of neural systems, vol. 26, no. 08, p. 1650043, 2016.

[5] F. He et al., "Nonlinear interactions in the thalamocortical loop in essential tremor: a model-based frequency domain analysis," Neuroscience, vol. 324, pp. 377–389, 2016.

[6] Y. T. Qassim, T. R. Cutmore, D. A. James, and D. D. Rowlands, "Wavelet coherence of EEG signals for a visual oddball task," Computers in Biology and Medicine, vol. 43, no. 1, pp. 23–31, 2013.

[7] S. Cheng, X. Chen, P. Xie, X. Pang, and X. Bai, "Functional Corticomuscular Coupling Based on Bivariate Empirical Mode Decomposition-Multiscale Transfer Entropy," in 2019 IEEE International Conference on Computational Intelligence and Virtual Environments for Measurement Systems and Applications (CIVEMSA), IEEE, 2019, pp. 1–4.

[8] T. Götz, L. Stadler, G. Fraunhofer, A. Tomé, H. Hausner, and E. Lang, "A combined cICA-EEMD analysis of EEG recordings from depressed or schizophrenic patients during olfactory stimulation," Journal of neural engineering, vol. 14, no. 1, p. 016011, 2016.

[9] K. Dragomiretskiy and D. Zosso, "Variational mode decomposition," IEEE transactions on signal processing, vol. 62, no. 3, pp. 531–544, 2013.

[10] N. ur Rehman and H. Aftab, "Multivariate variational mode decomposition," IEEE Transactions on signal processing, vol. 67, no. 23, pp. 6039–6052, 2019.

[11] D. Yi-Hao, Q. Wen-Jing, Z. Ce, Z. Jin-Ming, X. Bo-Duo, and X. Ping, "Intermuscular coupling characteristics based on variational mode decomposition-coherence," Acta Physica Sinica, vol. 66, no. 6, 2017.

[12] A. Duggento, L. Passamonti, G. Valenza, R. Barbieri, M. Guerrisi, and N. Toschi, "Multivariate Granger causality unveils directed parietal to prefrontal cortex connectivity during task-free MRI," Scientific reports, vol. 8, no. 1, pp. 1–11, 2018.

[13] L. A. Baccalá and K. Sameshima, "Partial directed coherence: a new concept in neural structure determination," Biological cybernetics, vol. 84, no. 6, pp. 463–474, 2001.

[14] K. J. Friston, "Functional and effective connectivity in neuroimaging: a synthesis," Human brain mapping, vol. 2, no. 1–2, pp. 56–78, 1994.

[15] G. V. Karanikolas, G. B. Giannakis, K. Slavakis, and R. M. Leahy, "Multi-kernel based nonlinear models for connectivity identification of brain networks," in 2016 IEEE International Conference on Acoustics, Speech and Signal Processing (ICASSP), IEEE, 2016, pp. 6315–6319.

[16] Q. Luo, T. Ge, F. Grabenhorst, J. Feng, and E. T. Rolls, "Attention-dependent modulation of cortical taste circuits revealed by Granger causality with signal-dependent noise," PLoS computational biology, vol. 9, no. 10, p. e1003265, 2013.

[17] E. Siggiridou and D. Kugiumtzis, "Granger causality in multivariate time series using a time-ordered restricted vector autoregressive model," IEEE Transactions on Signal Processing, vol. 64, no. 7, pp. 1759–1773, 2015.

[18] M. Staniek and K. Lehnertz, "Symbolic transfer entropy," Physical review letters, vol. 100, no. 15, p. 158101, 2008.

[19] T. Bossomaier et al., Transfer entropy. Springer, 2016.

[20] X. Chen et al., "Multiscale information transfer in functional corticomuscular coupling estimation following stroke: a pilot study," Frontiers in neurology, vol. 9, p. 287, 2018.

[21] X. Chen, Y. Zhang, S. Cheng, and P. Xie, "Transfer spectral entropy and application to functional corticomuscular coupling," IEEE Transactions on Neural Systems and Rehabilitation Engineering, vol. 27, no. 5, pp. 1092–1102, 2019.

[22] Y. Gao, L. Ren, R. Li, and Y. Zhang, "Electroencephalogram–electromyography coupling analysis in stroke based on symbolic transfer entropy," Frontiers in neurology, vol. 8, p. 716, 2018.

[23] R. Vicente, M. Wibral, M. Lindner, and G. Pipa, "Transfer entropy—a model-free measure of effective connectivity for the neurosciences," Journal of computational neuroscience, vol. 30, pp. 45–67, 2011.

[24] N. P. Subramaniyam, R. V. Donner, D. Caron, G. Panuccio, and J. Hyttinen, "Causal coupling inference from multivariate time series based on ordinal partition transition networks," Nonlinear Dynamics, vol. 105, no. 1, pp. 555–578, 2021.

[25] F. Takens, "Detecting strange attractors in turbulence," in Dynamical Systems and Turbulence, Warwick 1980: proceedings of a symposium held at the University of Warwick 1979/80, Springer, 2006, pp. 366–381.

[26] Y. Zou, R. V. Donner, N. Marwan, J. F. Donges, and J. Kurths, "Complex network approaches to nonlinear time series analysis," Physics Reports, vol. 787, pp. 1–97, 2019.

[27] E. M. Arnold, S. R. Ward, R. L. Lieber, and S. L. Delp, "A model of the lower limb for analysis of human movement," Annals of biomedical engineering, vol. 38, pp. 269–279, 2010.

[28] W. Omlor, L. Patino, M.-C. Hepp-Reymond, and R. Kristeva, "Gamma-range corticomuscular coherence during dynamic force output," Neuroimage, vol. 34, no. 3, pp. 1191–1198, 2007.

[29] M. Wibral et al., "Measuring information-transfer delays," PloS one, vol. 8, no. 2, p. e55809, 2013.

[30] W. Omlor, L. Patino, M.-C. Hepp-Reymond, and R. Kristeva, "Gamma-range corticomuscular coherence during dynamic force output," Neuroimage, vol. 34, no. 3, pp. 1191–1198, 2007.

[31] S. Slobounov, W. Ray, C. Cao, and H. Chiang, "Modulation of cortical activity as a result of task-specific practice," Neuroscience letters, vol. 421, no. 2, pp. 126–131, 2007.

[32] M. Zwarts, G. Bleijenberg, and B. Van Engelen, "Clinical neurophysiology of fatigue," Clinical neurophysiology, vol. 119, no. 1, pp. 2–10, 2008.

[33] J. Z. Liu et al., "Shifting of activation center in the brain during muscle fatigue: an explanation of minimal central fatigue?," Neuroimage, vol. 35, no. 1, pp. 299–307, 2007.

[34] B. Buchholz and T. J. Armstrong, "A kinematic model of the human hand to evaluate its prehensile capabilities," Journal of biomechanics, vol. 25, no. 2, pp. 149–162, 1992.

[35] W. Zeng, C. Yuan, Q. Wang, F. Liu, and Y. Wang, "Classification of gait patterns between patients with Parkinson's disease and healthy controls using phase space reconstruction (PSR), empirical mode decomposition (EMD) and neural networks," Neural Networks, vol. 111, pp. 64–76, 2019.

[36] X. Ping, F. Yang, X. Chen, and X. Wu, "EEG-EMG synchronization analysis based on gabor wavelet transform-granger causality," Chin J Biomed Eng, vol. 36, no. 1, pp. 28–38, 2017.

[37] X. Xi et al., "Analysis of Functional Corticomuscular Coupling Based on Multiscale Transfer Spectral Entropy," IEEE Journal of Biomedical and Health Informatics, vol. 26, no. 10, pp. 5085–5096, 2022.

[38] X. Chen, Y. Zhang, Y. Yang, X. Li, and P. Xie, "Beta-range corticomuscular coupling reflects asymmetries in hand movement," IEEE Transactions on Neural Systems and Rehabilitation Engineering, vol. 28, no. 11, pp. 2575–2585, 2020.

[39] I. M. de Abril, J. Yoshimoto, and K. Doya, "Connectivity inference from neural recording data: Challenges, mathematical bases and research directions," Neural Networks, vol. 102, pp. 120–137, 2018.

[40] F. B. Horak, "Assumptions underlying motor control for neurologic rehabilitation," in Contemporary management of motor control problems: Proceedings of the II STEP conference, Foundation for Physical Therapy Alexandria, Va, 1991, pp. 11–28.

[41] J. Liu, G. Tan, Y. Sheng, and H. Liu, "Multiscale transfer spectral entropy for quantifying corticomuscular interaction," IEEE Journal of Biomedical and Health Informatics, vol. 25, no. 6, pp. 2281–2292, 2020.

[42] P. Xie et al., "Analysis of abnormal muscular coupling during rehabilitation after stroke," Sheng wu yi xue Gong Cheng xue za zhi= Journal of Biomedical Engineering= Shengwu Yixue Gongchengxue Zazhi, vol. 33, no. 2, pp. 244–254, 2016.

[43] L. Chen, C. Zhang, X. Song, T. Zhang, X. Liu, and Z. Yang, "Construction and analysis of muscle functional network for exoskeleton robot," Sheng wu yi xue Gong Cheng xue za zhi= Journal of Biomedical Engineering= Shengwu Yixue Gongchengxue Zazhi, vol. 36, no. 4, pp. 565–572, 2019.

[44] Z. Wang and R. Suppiah, "Upper Limb Movement Recognition utilising EEG and EMG Signals for Rehabilitative Robotics," in Future of Information and Communication Conference, Springer, 2023, pp. 676–695.

Lantian Liu received the B.Eng. degree from the Anhui University of China, Hefei, China, in 2020, where she is currently pursuing the M.Eng. at Hangzhou Dianzi University, electronic information.

Her Research interests: Machine learning and brain-computer interface, biological information detection and processing.

Yunyuan Gao received her PhD in Control Theory and Control Engineering at Zhejiang University, China.

Currently she is a Professor in the School of Automation at Hangzhou Dianzi University, Hangzhou, China. Her Research interests: Machine learning and brain-computer interface, brain-computer hybrid intelligence, intelligent rehabilitation robots, biological information detection and processing.

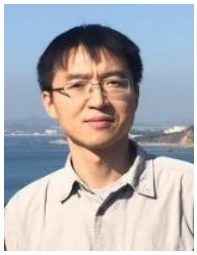

Ming Meng received his PhD in University of Science and Technology of China, China.

Currently he is an Associate Professor in the School of Automation at Hangzhou Dianzi University, Hangzhou, China. His Research interests: Machine learning and pattern recognition, brain-computer interface, motion gesture recognition.

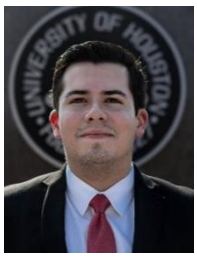

Michael Houston received his M.S. in Biomedical Engineering as well as Biology at the University of Houston.

He is currently a research assistant in the Department of Biomedical Engineering at the University of Houston, Houston, TX. His research interests include neural rehabilitation, multimodal neuroimaging, and brain-computer interfaces.

E-mail: mjhouston2@uh.edu

Yingchun Zhang received his PhD in Electrical Engineering at Zhejiang University, China, and completed his postdoctoral training in Biomedical Engineering at the University of Minnesota, Minneapolis, MN.

Currently he is a Professor in the Department of Biomedical Engineering at the University of Houston, Houston, TX. Dr. Zhang is a recipient of NIH Pathway to Independence (K99/R00) award and the 12th Annual Delsys Prize for Innovation in Electromyography. His research interests include multimodal neuroimaging and neural engineering, and neural rehabilitation.

E-mail: yingchun.umn@gmail.com